Role of Rare Earth Ion in Spin Glass Behavior for $R_{0.7}Sr_{1.3}MnO_4$

Chang Seop Hong,† Wan Seop Kim,† Eun Ok Chi,† Nam Hwi Hur,*,† and Yong Nam Choi‡

Center for CMR Materials, Korea Research Institute of Standards and Science, Yusong, P.O. Box 102, Taejon 305-600, Korea, and Neutron Physics Department, HANARO Center, Korea Atomic Energy Research Institute, Yusong, P.O. Box 105, Taejon 305-600, Korea

Received November 9, 2001. Revised Manuscript Received February 13, 2002

Magnetic and structural properties for melt-grown single crystals of monolayered manganites $R_{0.7}Sr_{1.3}MnO_4$ (R = La, Pr, and Nd), possessing the K_2NiF_4 type structure, have been investigated. On the bases of magnetization, neutron powder diffraction, and relaxation measurements, it is revealed that all the three compounds display spin glass behaviors in the low-temperature region. In $La_{0.7}Sr_{1.3}MnO_4$, spin glass behaviors are observed isotropically both in the *ab* plane and along the *c* axis. In contrast, $Pr_{0.7}Sr_{1.3}MnO_4$ and $Nd_{0.7}Sr_{1.3}MnO_4$ show anisotropic spin glass transition. The salient feature of spin glass behavior found in the Pr- and Nd-doped compounds can be understood in terms of the enhanced lattice distortion induced by small rare earth ion as well as the magnetic anisotropy of the rare earth ions.

Introduction

The doped perovskite manganite $R_{1-x}A_xMnO_3$ (R = rare earth, A = alkali earth) that shows colossal magnetoresitance (CMR) near the Curie temperature, T_C, has drawn considerable attention due to the potential application to magnetic devices.[1] The CMR effect is believed to be associated with the combined interplay among spin, charge, orbital, and lattice degrees of freedom.[2−4] To extend the fundamental knowledge of physics related to the CMR manganites, many efforts have also been made in other members of the Ruddlesdedn−Popper series $(R,A)_{n+1}Mn_nO_{3n+1}$. This is mainly because the physical property of this series compound depends on the dimensionality and thus can be easily tuned by varying *n*.[5,6] Particularly, the bi-layered manganite (*n* = 2) that consists of perovskite type layers intervened by a rock-salt [(R,A)O] layer exhibits very similar CMR behaviors as found in perovskite manganites.[7] It has been reported that the *n* = 2 member possesses diminished strength of magnetic interactions due to the reduced dimensionality, resulting in reduction of T_C of the bi-layered compound.[8−10] In addition, a comparative study between the two-dimensional $La_{1-x}Sr_{1+x}MnO_4$ system and the corresponding three-dimensional $La_{1-x}Sr_xMnO_3$ system by Mohan Ram et al. revealed that increasing the number of perovskite layers causes an increase in electrical conductivity as well as ferromagnetic interaction.[11]

On the other hand, the pronounced CMR concomitant with long-range ferromagnetic ordering found in the *n* = ∞ and 2 phases is generally absent in the monolayered manganite (*n* = 1).[12−14] Instead, the *n* = 1 member has been known to show intriguing physical phenomena such as charge, orbital, and spin orderings.[15,16] To gain insight into that feature, initial research has been focused on the 50% doped sample $R_{0.5}Sr_{1.5}MnO_4$, where Mn^{3+} and Mn^{4+} exist as an equal ratio.[17−19] The charge and orbital orderings of interest were observed in $La_{0.5}Sr_{1.5}MnO_4$, which are melted under pulsed magnetic fields up to 40 T.[20] The existence of orbital ordering was

* Corresponding author. E-mail: nhhur@kriss.re.kr.
† Korea Research Institute of Standards and Science.
‡ Korea Atomic Energy Research Institute.

(1) Jin, S.; Tiefel, T. H.; McCormack, M.; Fastnacht, R. A.; Ramesh, R.; Chel, H. *Science* **1994**, *264*, 413.
(2) Endoh, Y.; Hirota, K.; Ishihara, S.; Pkamoto, S.; Murakami, Y.; Nishizawa, A.; Fukuda, T.; Kimura, H.; Nojiri, H.; Kaneko, K.; Maekawa, S. *Phys. Rev. Lett.* **1999**, *82*, 4328.
(3) Uhlenbruck, S.; Teipen, R.; Klingeler, R.; Büchner, B.; Friedt, O.; Hücker, M.; Kierspel, H.; Niemöller, T.; Pinsard, L.; Revcolevschi, A.; Gross, R. *Phys. Rev. Lett.* **1999**, *82*, 185.
(4) Hong, C. S.; Kim, W. S.; Hur, N. H. *Phys. Rev. B* **2001**, *63*, 092504.
(5) Witte, N. S.; Goodman, P. G.; Lincoln, F. J.; March, R. H.; Kennedy, S. J. *Appl. Phys. Lett.* **1998**, *72*, 853.
(6) Asano, H.; Hayakawa, J.; Matsui, M. *Appl. Phys. Lett.* **1997**, *71*, 844.
(7) Chi, E. O.; Kwon, Y.-U.; Kim, J.-T.; Hur, N. H. *Solid State Commun.* **1999**, *110*, 569.
(8) Hong, C. S.; Kim, W. S.; Chi, E. O.; Lee, K. W.; Hur, N. H. *Chem. Mater.* **2000**, *12*, 3509.
(9) Hur, N. H.; Kim, J.-T.; Yoo, K. H.; Park, Y. K.; Park, J.-C.; Chi, E. O.; Kwon, Y. U. *Phys. Rev. B* **1998**, *57*, 10740.
(10) Moritomo, Y.; Itoh, M. *Phys. Rev. B* **1999**, *59*, 8789.
(11) Mohan Ram, R. A.; Ganguly, P.; Rao, C. N. R. *J. Solid State Chem.* **1987**, *70*, 82.
(12) Moritomo, Y.; Tomioka, Y.; Asamitsu, A.; Tokura, Y. *Phys. Rev. B* **1995**, *51*, 3297.
(13) Bao, W.; Chen, C. H.; Carter, S. A.; Cheong, S.-W. *Solid State Commun.* **1996**, *98*, 55.
(14) Li, R. K.; Greaves, C. *J. Solid State Chem.* **2000**, *153*, 34.
(15) Sternlieb, B. J.; Hill, J. P.; Wildgruber, U. C.; Luke, G. M.; Nachumi, B.; Moritomo, Y.; Tokura, Y. *Phys. Rev. Lett.* **1996**, *76*, 2169.
(16) Murakami, Y.; Kawada, H.; Kawata, H.; Tanaka, M.; Arima, T.; Moritomo, Y.; Tokura, Y. *Phys. Rev. Lett.* **1998**, *80*, 1932.
(17) Hong, C. S.; Chi, E. O.; Kim, W. S.; Hur, N. H.; Lee, K. W.; Lee, C. H. *Chem. Mater.* **2001**, *13*, 945.
(18) Moritomo, Y.; Nakamura, A.; Mori, S.; Yamamoto, N.; Ohoyama, K.; Ohashi, M. *Phys. Rev. B* **1997**, *56*, 14879.
(19) Park, J.; Lee, S.; Park, J.-G.; Swainson, I. P.; Moritomo, Y.; Ri, H.-C. *Phys. Rev. B* **2000**, *62*, 13848.

10.1021/cm0115618 CCC: $22.00
Published on Web 03/21/2002

identified using synchrotron X-ray diffraction study by Murakami et al.[16] Recently, Moritomo et al. studied the $La_{1-x}Sr_{1+x}MnO_4$ ($0.0 \le x \le 0.7$) compounds and reported that the spin glass phase exists between $x = 0.2$ and 0.6.[12] In the La-doped manganites the spin glass state is present in the wide doping range, which is possibly due to the competing interaction between ferromagnetic (FM) and antiferromagnetic (AFM) states. To understand the effect of the rare earth ion, instead of the doping concentration, on spin glass sate observed in the monolayered manganite system, we have investigated structural and physical properties of $R_{0.7}Sr_{1.3}MnO_4$ (R = La, Pr, and Nd; hereafter denoted as R-214) that has the 30% doping level nominally.

In this paper we present synthesis, magnetic, and structural properties of single crystals of R-214 that are grown by the floating zone method, together with neutron diffraction result. Particularly, we put more emphasis on Nd-214 of which the structural variation with temperature and the remnant magnetization are investigated to elucidate the anisotropic magnetic nature found in the Pr- and Nd-doped materials. In addition, structural comparison between Nd-214 and $Nd_{0.5}Sr_{1.5}MnO_4$ was also made to manipulate the effect of doping level on this system.[17] Our studies reveal that both magnetic anisotropy and reduced ionic radius of rare earth ion play crucial role in determining the anisotropic spin glass behavior in Pr-214 and Nd-214.

Experimental Section

Polycrystalline powders of R-214 (R = La, Pr, and Nd) grown for single crystals were prepared using conventional solid-state reaction method. A stoichiometric mixture of corresponding rare earth oxide, $SrCO_3$, and MnO_2 was calcined at 1000 °C for 24 h in air. The calcined samples were pulverized, pelletized, and sintered at 1300 °C for 60 h with intermediate grinding. The resultant pellet was ground to powders, which were then cold-pressed to make a cylindrical shaped rod (6 mm × 80 mm = diameter × length). The rod was sintered at 1450 °C for 20 h in air.

Single crystals of R-214 were grown in flowing oxygen using a floating zone image furnace (Crystal Systems, Inc.) equipped with four mirrors and four halogen lamps with total input power of 4 kW. The oxygen flow rate was 2.5 L/min. Both feed and seed rods were coaxially rotated in opposite directions at a rate of 25 rpm. The growth rate was 13 mm/h. The temperature of the molten zone was measured by detecting blackbody radiation of graphite rod with a pyrometer. The temperatures of the focused areas for the R-214 samples were around 1860 °C. All the three crystals were grown under very similar conditions.

Samples for the measurements are cleaved from the resulting boule about 5 mm in diameter and 50 mm in length that contains many single crystals. Electron-probe microanalysis on the R-214 crystals confirmed that starting nominal compositions are maintained in all the three crystals. Crystals from the boule were crushed into powders for X-ray and neutron diffraction measurements. The X-ray diffraction data were scanned in $10° \le 2\theta \le 120°$ with a step size of 0.02° using a Rigaku RAD diffractometer equipped with Cu Kα radiation. Neutron diffraction data were recorded over the 2θ range of 0° to 160° with a step size of 0.05° on a HRPD (high-resolution powder diffractometer) at HANARO Center in KAERI, where a neutron source with $\lambda = 1.8348$ Å supplied by Ge(331) single-crystal monochromator was used. The diffraction data were analyzed by Rietveld profile analysis based on Fullprof program.[21] For magnetic property measurements the single crystals of R-214 (R = La, Pr, and Nd) were cleaved in the longitudinal direction due to their anisotropic nature. The cleaved surface was checked by the XRD patterns having (00*l*) peaks only, indicating that the surface lies in the *ab* plane. The magnetization measurements were performed using a Quantum Design MPMS-5 SQUID magnetometer and a physical property measurement system (PPMS-7) magnetometer, where fields are applied parallel to the *ab* plane and along the *c* axis. Electrical resistivity was measured as a function of temperature using the standard four-probe method with and without magnetic field. The four-point contacts were made with molten indium on the *ab* plane of the crystals.

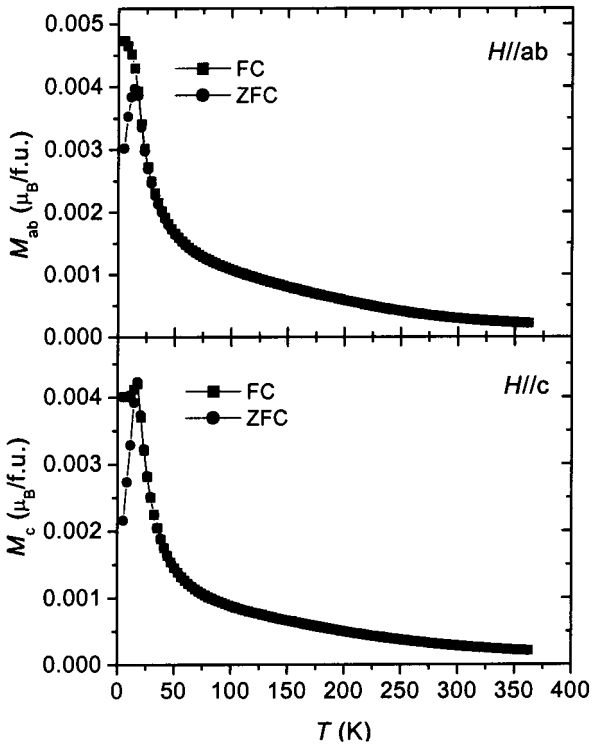

Figure 1. Temperature dependence of the magnetization measured with *H* parallel to the *ab* plane (top) and along the *c* axis (bottom) for La-214, where the applied magnetic field is 100 G.

Results and Discussion

To assess the role of rare earth ion in magnetic properties of the monolayered manganites R-214, we measured their temperature-dependent magnetizations at 100 G in which magnetic field is applied parallel to the *c* axis and the *ab* plane as displayed in Figures 1−3. Their magnetic data together with structural parameters are summarized in Table 1. Figure 1 shows the temperature dependence of magnetization curves for La-214 in both directions. The magnetization value M_{ab} parallel to the *ab* plane increases gradually with decreasing temperature and reaches a cusp at about 17 K. Below this temperature, the zero-field-cooled (ZFC) and field-cooled (FC) magnetization curves are split, which is characteristic of a spin glass transition. Hereafter, the cusp temperature in the ZFC magnetization curve denotes as T_{SG}.[22] Similar magnetic behavior,

(20) Tokunaga, M.; Miura, N.; Moritomo, Y.; Tokura, Y. *Phys. Rev. B* **1999**, *59*, 11151.

(21) Roisnel, T.; Rodríguez-Carvajal, J. *Program: Fullprof*; LLB-LCSIM: France, 2000.

(22) Mathieu, R.; Jönsson, P.; Nam, D. N. H.; Nordblad, P. *Phys. Rev. B* **2001**, *63*, 92401.

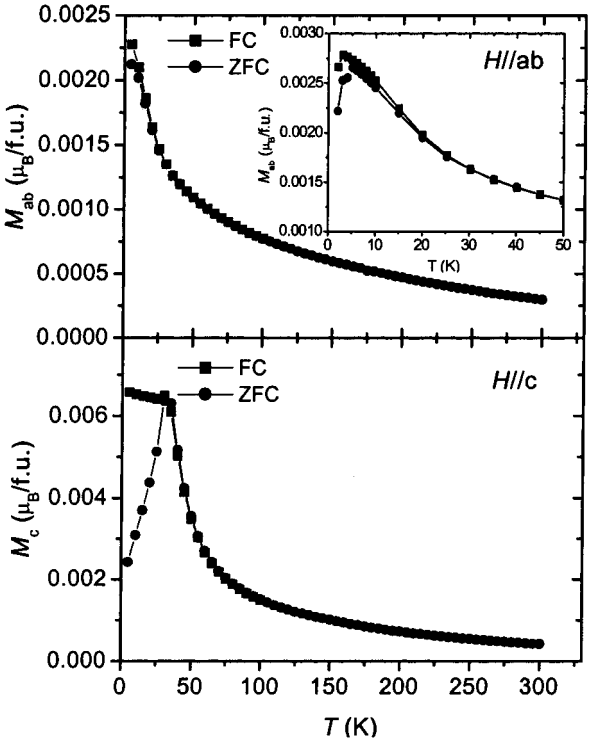

Figure 2. Magnetization versus temperature curves for Pr-214. Top part shows the in-plane magnetization curve and bottom one exhibits the magnetization curve measured along the *c* axis, where the applied magnetic field is 100 G.

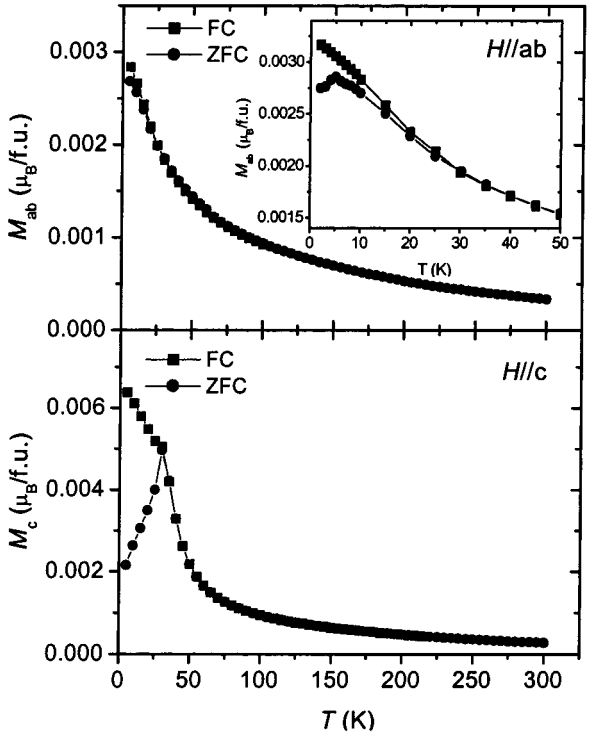

Figure 3. Temperature dependence of the magnetization measured with *H* parallel to the *ab* plane (top) and along the *c* axis (bottom) for Nd-214. Here the applied magnetic field is 100 G.

although the magnetization value of M_c is slightly smaller than M_{ab}, is found in the M_c versus T curve shown in bottom panel of Figure 1. For R-214 it is interesting to note that the $M(T)$ data obey the Curie−Weiss law in a high-temperature region. The calculated

Table 1. Mean Radius of *A* Site ($\langle r_A \rangle$), Tolerance Factor (t), Jahn−Teller Distortion (D), Spin Glass Freezing Temperature (T_{SG}), and Coercive Field (H_C) in R-214[a]

		R			
		La	Pr	Nd	$Nd_{0.5}$
$\langle r_A \rangle$ (Å)		1.4171	1.4042	1.3986	1.4133
t		0.942	0.937	0.935	0.951
D		1.06	1.08	1.08	1.05
T_{SG} (K)	*ab* plane	17	5	5	21
	c axis	17	30	30	21
H_C(G)	*ab* plane	280	70	160	400
	c axis	700	2800	4200	800

[a] $Nd_{0.5}$ stands for $Nd_{0.5}Sr_{1.5}MnO_4$.

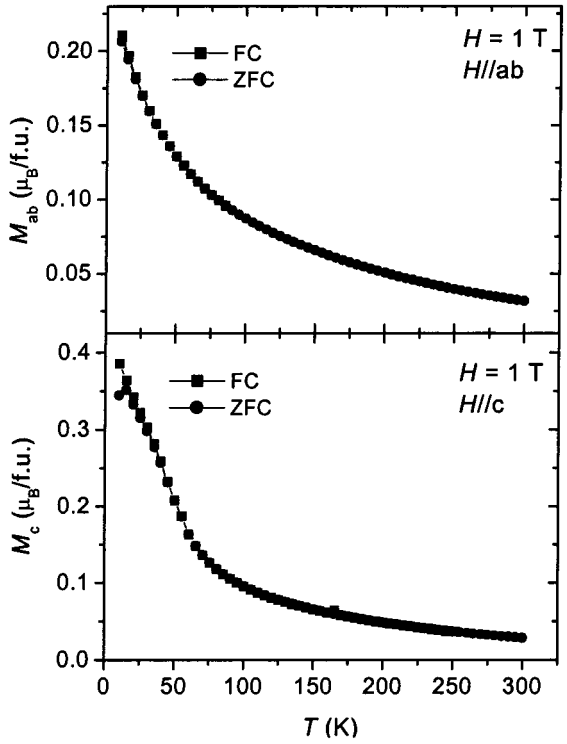

Figure 4. Temperature dependence of the magnetization measured with *H* parallel to the *ab* plane (top) and along the *c* axis (bottom) for Nd-214. Here the applied magnetic field is 1 T.

Weiss constants in the range of 43 K − 127 K agree well with those found in the La-doped samples $La_{1+x}Sr_{1-x}MnO_4$ ($0 \le x \le 0.7$).[12] This implies that there exist some ferromagnetic components presumably originated from the double exchange interaction between the Mn^{3+} and Mn^{4+} ions,[12] which is also evidenced by the magnetization hysteresis data of La-214 at 5 K shown in the top part of Figure 5. As illustrated in the hysteresis curves, weak coercive fields of 280 and 700 G are found in the *ab* plane and along the *c* axis, respectively. The magnetization values of the *ab* plane and the *c* axis at 5 T are estimated to be 0.86 μ_B and 0.77 μ_B, respectively, which are much smaller than the theoretical value (3.7 μ_B) for full FM alignment of Mn ions, designating the presence of AFM state. It is thus conceivable that the spin glass transition arises from the competition between AFM interaction induced by the superexchange pathway and FM alignment derived from the double exchange route.[23]

(23) Nam, D. N. H.; Mathieu, R.; Nordbland, P.; Khiem, N. V.; Phuc, N. X. *Phys. Rev. B* **2000**, *62*, 1027.

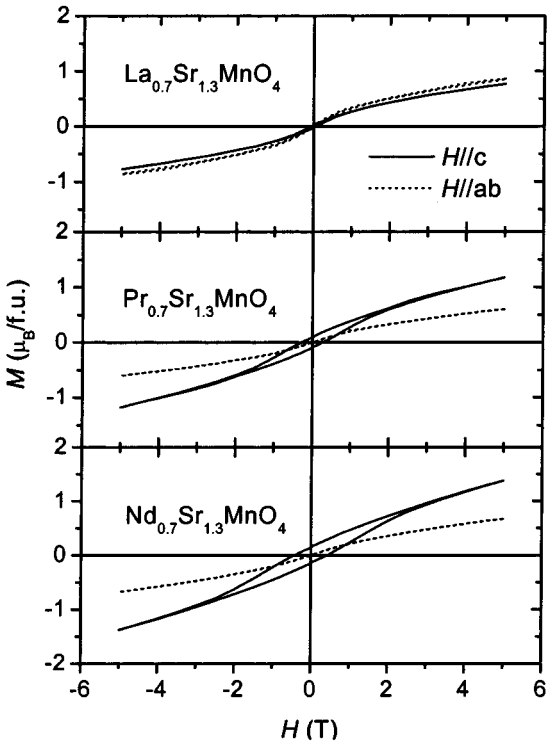

Figure 5. *M* versus *H* for R-214, where R is La (top), Pr (middle), and Nd (bottom). The samples were measured at 5 K with *H* parallel to the *ab* plane and along the *c* axis. Dashed lines represent the *M*(*H*) curve measured parallel to the *ab* plane. Solid lines correspond to the *M*(*H*) curve measured along the *c* axis.

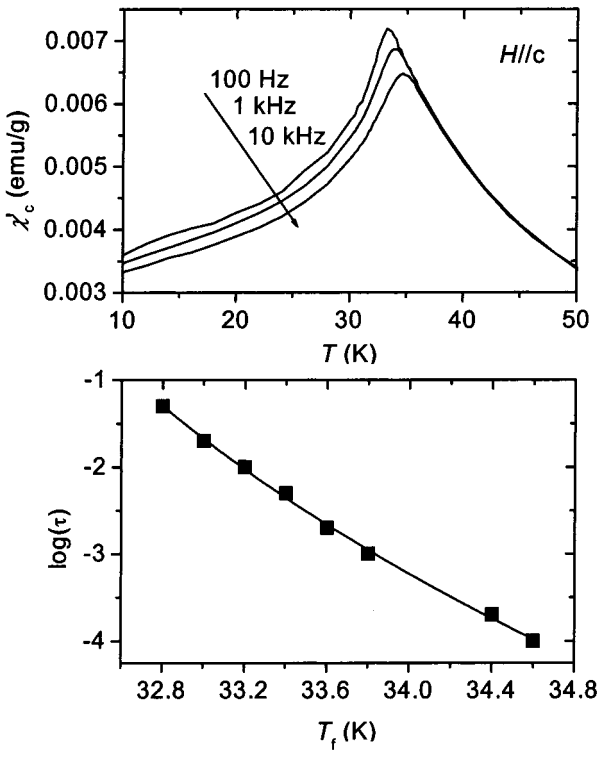

Figure 6. Real part (χ'_c) of ac magnetic susceptibility for Nd-214 under an ac field of 10 G at different frequencies along the *c* axis (top) and the best fit of the log(τ) data to the critical slowing down eq (bottom) as a function of T_f.

The spin glassy phenomenon is also observed in Pr- and Nd-214, which may take place due to magnetic frustration and randomness.[24] The magnetic frustration becomes realized because the involvement of magnetic moment of rare earth ion (R) into the AFM background formed by interactions among Mn ions generates competing magnetic interactions among R−R, R−Mn, and Mn−Mn, which results in a magnetic frustration. The site randomness is due to the fact that the magnetic R^{3+} and nonmagnetic Sr^{2+} ions are randomly distributed over the same cystallographic sites. Unlike La-214, however, Pr-214 and Nd-214 show distinctive disparity in magnetic transitions in the temperature-dependent magnetization curves. As shown in Figure 2, $M_c(T)$ for Pr-214 exhibits a spin glass transition at about 30 K but a cusp in the ZFC curve in the *ab* plane goes down to 5 K. By comparison with La-214, this feature seems to be associated with the magnetic anisotropy of the magnetic rare earth ion. As anticipated from almost identical ionic radius and magnetic moment of Nd^{3+} and Pr^{3+} ions, the *M*(*T*) curve of Nd-214 given in Figure 3 shows very similar magnetic behavior to that for the Pr-214 sample. Figure 4 illustrates that applying a higher magnetic field of $H = 1$ T to Nd-214 changes the cusp of M_c down to 15 K, freezing the magnetic state at a lower temperature. Interestingly, the axis-dependent behavior disappears in the 50% doped sample $Nd_{0.5}Sr_{1.5}MnO_4$ where the spin glass transition is found in the *c* axis as well as along the *ab* plane at an identical temperature.[17] This implies that the spin glass state is also sensitive to the doping level of the R ion. A plausible cause for the characteristic magnetism depending on the axis will be discussed below on the basis of structural data.

Another noticeable point in the *M*(*T*) curves of the Pr- and Nd-doped samples is that the magnetization values along the *c* axis are larger than those in the *ab* plane, which is consistent with the field dependent magnetization data as depicted in middle and bottom panels of Figure 5. The magnetization at 5 T along the *c* axis and in the *ab* plane for Pr-214 is 1.19 μ_B and 0.60 μ_B, respectively. Similar behavior is observed in Nd-214, in which the magnetization magnitudes along the *c* axis and in the *ab* plane are 1.38 μ_B and 0.68 μ_B, respectively. It is noticed that the out-of-plane magnetizations in Pr- and Nd-214 are significantly enhanced while the in-plane magnetizations slightly diminish with respect to those of La-214. These results suggest that the rare earth moments mostly contribute to the *c* axis magnetization and Mn spins tend to slightly rotate toward the *c* axis. The *c* axis magnetization values of Pr- and Nd-214 are smaller than the theoretical ones (2.24 μ_B for R = Pr and 2.29 μ_B for R = Nd) deduced from FM saturation magnetization of the rare earth spins, implying that the rare earth spins are frustrated and correlated with the Mn spins. The coercive field also shows anisotropic characteristics in both Pr-214 and Nd-214. For Pr-214, coercive fields of the *c* axis and the *ab* plane are 2800 and 70 G, respectively. Similarly, Nd-214 has coercive fields of 4200 G (*c* axis) and 160 G (*ab* plane). These anisotropic behaviors appear to be associated with the presence of magnetic rare earth ions.

The magnetic nature of Nd-214 was also examined by means of ac susceptibility along the *c* axis and in the *ab* plane. Figure 6 shows the temperature depen-

(24) Binder, K.; Young, A. P. *Rev. Mod. Phys.* **1986**, *58*, 801.

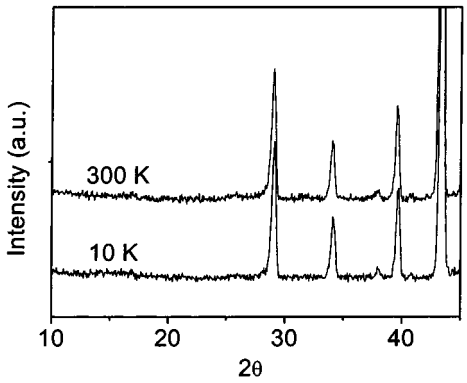

Figure 7. Neutron powder diffraction patterns of Nd-214 at 10 and 300 K in the low 2θ region.

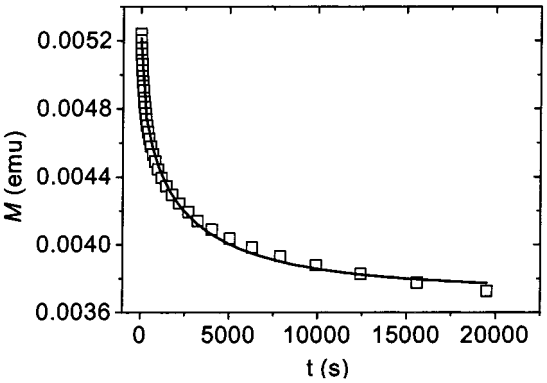

Figure 8. Time dependence of the remnant magnetization for Nd-214 at 10 K. A magnetic field of 5 T was applied parallel to the *c* axis. The solid line is a fitting curve.

dence of the real part (χ'_c) at various frequencies along the *c* axis. The frequency dependent maximums in χ'_c-(T), often taken as a sign of spin glass system, are observed. The dynamical slowing down for spin glasses can be expressed as $\tau/\tau_0 = [T_f/T_G - 1]^{-z\nu}$ where τ is the relaxation time, τ_0 the shortest relaxation time, T_f the freezing temperature, T_G the spin glass temperature, and $z\nu$ the critical exponent. The bottom part of Figure 6 shows that the best fit affords parameters of $\tau_0 = 1.6 \times 10^{-14}$ s, $T_G = 30$ K, and $z\nu = 11.9$. The obtained τ_0 value falls into the range of spin glasses and the $z\nu$ one is almost identical to that of spin glass phase $Ho_5Co_{50}Al_{45}$.[25−27] Another quantity for spin glasses is computed using the formula $K = \Delta T_f/[T_f \Delta \ln(f)]$ where K for spin glasses is found to be of the order of 0.01.[25] The calculated value of $K = 0.009(1)$ in this system agrees well with the spin glass category. Likewise, the frequency-dependent behaviors are found in La-214 and Pr-214 with T_G of 15 and 32 K, respectively. In the *ab* plane, the ac susceptibility data for R-214 also show frequency dependence around T_{SG}.

To evaluate the spin glass nature found in Nd-214, we investigated its temperature-dependent structural change and remnant magnetization in more detail. Figure 7 displays the neutron powder diffraction patterns for Nd-214 at 10 and 300 K. Neither superlattice reflections nor enhanced intensities of nuclear peaks are detected in both neutron diffraction data, suggesting that there is little evidence of long-range magnetic ordering in Nd-214. This consequence thus confirms that the cusp at 30 K in the $M(T)$ curve for Nd-214 can be considered as the onset of a spin glass transition. Figure 8 exhibits the remnant magnetization data of Nd-214, which were collected by applying a magnetic field of 5 T parallel to the *c* axis. The relaxation effect is evident below T_{SG}, ensuring the existence of spin glass state in Nd-214. The magnetization data decayed exponentially were fitted with the stretched equation $M = M_f + (M_i - M_f)\exp[-(t/\tau)^{\beta}]$, where M_i and M_f denote the initial and final magnetization magnitudes, respectively. The symbols t and τ are the delay time and the relaxation constant, respectively. The β value varies from 0 (no relaxation) to 1 (conventional Debye relaxation).[28] From the fitting curve we found that τ is 1.84(5) $\times 10^3$ s and β is 0.54(1), simply reflecting the presence of the spin glass state in that many energy valleys subsist.[29]

Table 2. Lattice Parameters for R-214 at 300 K Based on XRD Data

R	*a* (Å)	*c* (Å)	*V* (Å^3)
La	3.8545(1)	12.6006(2)	187.207(5)
Pr	3.8329(1)	12.5525(2)	184.414(5)
Nd	3.8284(1)	12.5165(3)	183.453(8)

Now we turn our attention to the anisotropic behavior of the spin glass state in the Pr- and Nd-doped compounds and its correlation with structure. To understand this feature, we analyzed variations in cell parameters, bond length, bond angle, and Jahn−Teller distortion of R-214 and particularly investigated structural change of Nd-214 with temperature. The XRD data of R-214 were indexed with the space group *I*4/*mmm*, where lattice parameters are given in Table 2. As expected from the mean radius of the R/Sr site, the lattice constants are almost linearly contracted with decreasing the radius. Tolerance factors of La-214 and Nd-214 are 0.942 and 0.935, respectively, implying that Nd-214 experiences more distortion. To investigate the structural change in Nd-214 with temperature, we measured neutron diffraction patterns for Nd-214 at some selected temperatures. Figure 9 exhibits the temperature evolution of cell parameters obtained from the Rietveld refinements. The cell volume has shrinkage of 0.64% with decreasing temperature from 300 to 10 K. At the same time, the *a* and *c* axes decrease by about 0.20% and 0.23%, respectively.

Figure 10 illustrates the variations of the Mn−O bond lengths and the Jahn−Teller distortion (D) in Nd-214 with temperature in which D is defined as d_{Mn-O2}/d_{Mn-O1}. Here, d_{Mn-O1} stands for the equatorial Mn−O bond distance and d_{Mn-O2} represents the axial Mn−O bond length. As can be clearly seen in the top part of Figure 10, the Mn−O1 bond length almost linearly decreases down to 40 K and holds at that distance below 40 K. In contrast, the axial Mn−O2 bond length reduces down to 100 K and below the temperature increases smoothly. The Jahn−Teller distortion (D) remains

(25) Greedan, J. E.; Raju, N. P.; Maignan, A.; Simon, Ch.; Pedersen, J. S.; Niraimathi, A. M.; Gmelin, E.; Subramanian, M. A. *Phys. Rev. B* **1996**, *54*, 7189.
(26) Laiho, R.; Lahderanta, E.; Salminen, J.; Lisunov, K. G.; Zakhvalinskii, V. S. *Phys. Rev. B* **2001**, *63*, 094405.
(27) Tholence, J. L. *Phys. B* **1984**, *126*, 157.
(28) Palmer, R. G.; Stein, D. L.; Abrahams, E.; Anderson, P. W. *Phys. Rev. Lett.* **1984**, *53*, 958.
(29) Gönen, Z. S.; Fournier, P.; Smolyaninova, V.; Greene, R.; Araujo-Moreira, F. M.; Eichhorn, B. *Chem. Mater.* **2000**, *12*, 3331.

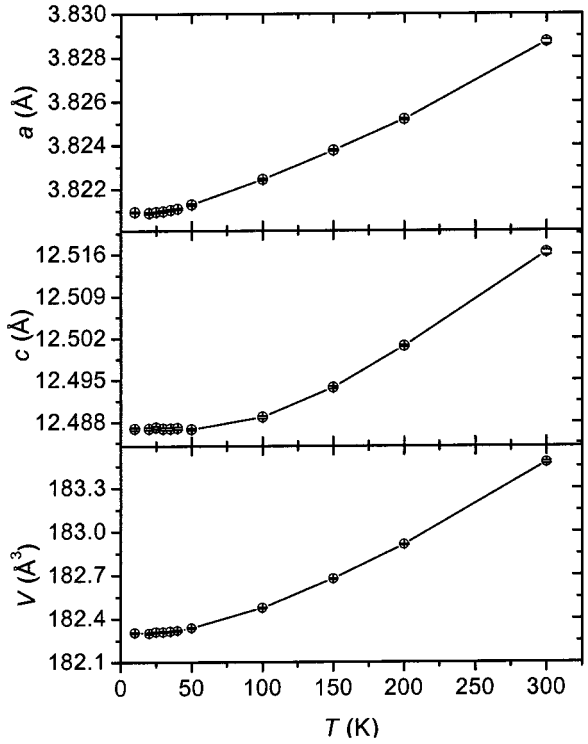

Figure 9. Unit cell parameters of *a* (top) and *c* axes (middle) for Nd-214 as a function of temperature. The temperature dependence of the unit cell volume for Nd-214 is shown in the bottom part.

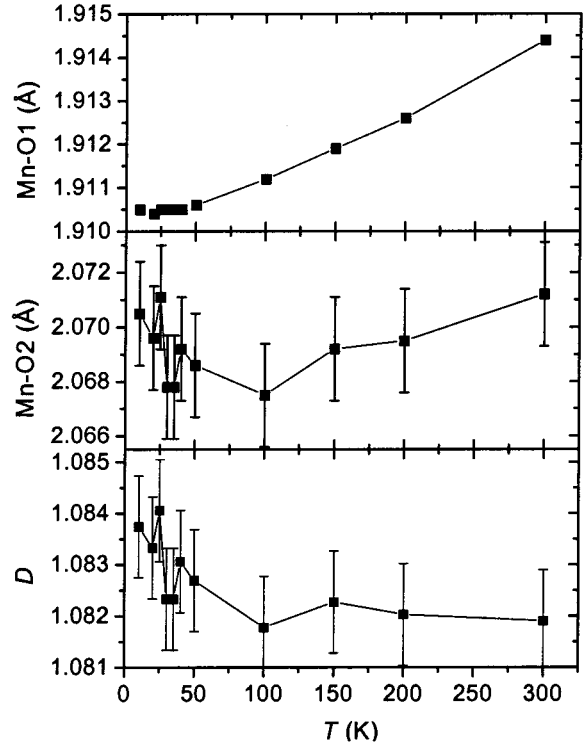

Figure 10. Top and middle parts show the temperature dependence of the equatorial Mn−O1 and axial Mn−O2 bond lengths for Nd-214. The Jahn−Teller distortion (*D*) as a function of temperature for Nd-214 is displayed in the bottom part.

almost unchanged down to 100 K and increases on further cooling. The axial bond length shows very small drop at 30 K close to T_{SG}, which might indicate that the spin glass transition in Nd-214 is correlated with

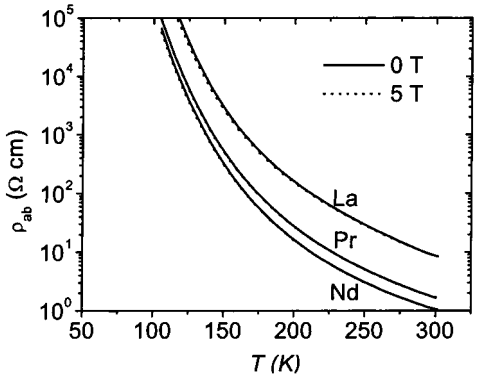

Figure 11. Temperature dependence of in-plane resistivity for R-214 (R = La, Pr, and Nd). Solid and doted lines represent the resistivity curves at 0 and 5 T, respectively.

the structural change. This is consistent with the observation in $Nd_{0.5}Sr_{1.5}MnO_4$.[17] As given in Table 1, the *D* values at 300 K for Nd-214 and $Nd_{0.5}Sr_{1.5}MnO_4$ are 1.08 and 1.05, respectively, which gives an explanation on the observed magnetic differences in spin glass transition between them. Similarly, at the same doping level the size of rare earth ion alters the distortion magnitude as exemplified by *D* values of 1.08 for Pr-214 and 1.06 for La-214. Note that Pr-214 and Nd-214 have the same values of *D*, allowing them to have similar magnetic behaviors. Thus, the replacement of R = La with R = Pr or Nd in the R-214 phase affords an increased *D* value, signaling the system becomes more anisotropically distorted.

Based on the magnetic and structural data described above, the structural anisotropy evidenced by the tolerance factors and Jahn−Teller distortion values as illustrated in Table 1 is one of the most likely cause of the magnetic anisotropy seen in the Pr- and Nd-doped samples. The magnetic moment of the rare earth ion whose magnetic anisotropy is strong appears to be stabilized axially under a given environment that can be established by the structural anisotropy in the Pr- and Nd-214 system. Moreover, the structural distortion is likely to perturb the robust AFM matrix by lowering energy level of d_{z^2} orbital rather than $d_{x^2-y^2}$ level. Consequently, this allows Mn spins to be coupled with the rare earth magnetic spins, forcing Mn spins to be oriented more toward the *c* direction. This conjecture is consistent with the *M*(*T*) and *M*(*H*) results. These interactions eventually make T_{SG} shift to higher temperature in the *c* axis magnetization as seen in Pr- and Nd-214. The enhanced T_{SG} is also associated with the lattice contraction driven by the Pr- or Nd-doping that has reduced ionic radius. It is hence evident that both the structural anisotropy of the system and the magnetic anisotropy of the rare earth ion are responsible for the magnetic anisotropy of spin glass transition in the monolayered manganites.

Figure 11 shows the temperature dependence of in-plane resistivity (ρ_{ab}) for R-214. The higher resistivity in La-214 than the reported result by Moritomo et al.[12] may arise from possible defects in this sample. As temperature decreases, ρ_{ab} continuously increases and finally diverges at low temperatures. This insulating behavior is typical of monolayered manganites, demonstrating that itinerant electrons are unable to hop easily from one site on a Mn atom to the other on a neighbor-

ing Mn atom. This is likely due to the fact that on condition of increasing D with temperature, shown in bottom panel of Figure 10, d_{z^2} orbitals in e_g levels of Mn^{3+}/Mn^{4+} ions have lower energy states than $d_{x^2-y^2}$ orbitals. This situation would force itinerant electrons moving around via $d_{x^2-y^2}$ orbitals in the plane to be localized on d_{z^2} orbitals, leading to the insulating state. The resistivity data are well fitted with the small-polaron hopping equation $\rho = AT \exp(E_a/k_B T)$, yielding an activation energy of 170 meV for La-214, 167 meV for Pr-214, and 168 meV for Nd-214. The magnitude of ρ_{ab} decreases when Pr or Nd substitutes La in R-214, implicating the improvement of electrical transport. The in-plane resistivity is likely to be controlled by the hoping on Mn atoms. This enhanced conduction process may take place because the introduced rare earth ions and structural distortion slightly perturb the AFM character, which in turn allows electrons to hop rather easily. The application of a magnetic field of 5 T induced a tiny suppression of resistivity where magneto resistance defined as $(\rho_H - \rho_0)/\rho_0$ reaches to 10% at 150 K. Here ρ_0 stands for the resistivity at zero magnetic field and ρ_H at 5 T. The enhanced spin alignment induced by the external magnetic field is responsible for the small MR effects.[17]

Conclusions

We have successfully grown single crystals of the monolayered manganites R-214 (R = La, Pr, and Nd), and investigated their magnetic, structural, and transport properties. All the three manganites are insulating and undergo spin glass transitions. An important finding is that La-214 exhibits the spin glass transitions at the same temperature regardless of the axis while the Pr- and Nd-doped samples show the anisotropic spin glass transition with the large difference in spin-glass temperatures. Our comprehensive set of structural and magnetic data clearly reveals that the unique anisotropic magnetic properties found in Pr-214 and Nd-214 are due to both the structural and magnetic anisotropies induced by the magnetic rare earth ion. These results provide new perspective to understand the monolayered manganites where the rare earth ion plays an important role in determining the magnetic property. The induced magnetic anisotropy may be utilized to generate ferromagnetism in the two-dimensional magnetic system.

Acknowledgment. We wish to thank Prof. J. G. Park and Dr. J. Dho for helpful comments. The Creative Research Initiative Program financially sponsored this work.

CM0115618